or (DPA)FeOFe(DPA) does not result in O_2 evolution, but yields stable HOOH adducts (Figure 3 and 4). In contrast to free HOOH, which is oxidized at +1.25 V vs SCE, the adducts are oxidized at +1.00 V (Table I). In a recent investigation,[12] the $(PA)_2FeOFe(PA)_2$ and (DPA)FeOFe(DPA) complexes in a 2:1 py/HOAc solvent system have been shown to activate HOOH for the selective dioxygenation of PhC≡CPh to PhC(O)C(O)Ph and the direct transformation of cyclohexane to cyclohexanone (95%, with 5% c-$C_6H_{11}OH$). On the basis that (a) $^1O_2$ is evolved when $(PA)_2FeOFe(PA)_2$ and HOOH are combined in DMF, (b) $(PA)_2FeOFe(PA)_2$ and HOOH form a stable adduct (**2**, Scheme I) in 2:1 py/HOAc, and (c) in the presence of the latter system, PhC≡CPh undergoes dioxygenation, we conclude that there is a common reactive intermediate $[(PA)_2FeO(OO)Fe(PA)_2$ (**3**) (and (DPA)FeOOFe(DPA) for the (DPA)FeOFe(DPA)/HOOH system)].[12]

The reductions of $Fe^{III}(DPA)^+$ in the absence and presence of O_2, which are illustrated by the voltammograms of Figure 5 and the ring-disk current-voltage curves of Figure 6, indicate that an easily reduced intermediate is formed [probably (DPA)FeOO•; $E_{p,c}$ = +0.4 V vs SCE]. This potential is the same as that for the reduction of HOO• in DMF,[17] which is reasonable for electron addition to a peroxy radical formulation, (DPA)FeOO•. Scheme Ic outlines a self-consistent reaction sequence for the hydrolytic dimerization of $Fe^{III}(DPA)^+$, and Scheme Id outlines the reaction intermediates when O_2 is present. With excess $Fe^{II}(DPA)$ present, the (DPA)FeOO• intermediate is immediately transformed to (DPA)FeOFe(DPA) (**4**). If excess 1,4-cyclohexadiene (1,4-CHD) is present, the peak at −0.22 V (Figure 5) is not observed because the (DPA)FeOO• intermediate reacts with the allyl hydrogen atoms of 1,4-CHD.

In pyridine/acetic acid solvent, $Fe^{II}(DPAH)_2$ in the presence of O_2 and excess substrate is autoxidized to a reactive intermediate, which ketonizes methylene carbons and dioxygenates acetylenes, aryl olefins, and catechols.[14] Because the products are identical with those that result from the reactive intermediate formed from the combination of (DPA)FeOFe(DPA) and excess HOOH, (DPA)FeOOFe(DPA),[12] the dioxygenation of the substrates must result from a similar reactive intermediate. The close parallels of the product profiles as well as the results of the kinetic measurements prompt the conclusion that the combination of $Fe^{II}(DPA)_2$ and O_2 results in the initial formation of the reactive intermediate $(DPAH)_2FeOOFe(DPAH)_2$ via a rate-limiting step. In the absence of substrate, the active catalyst is rapidly autoxidized to $(DPAH)_2FeOFe(DPAH)_2$, which is reduced to $Fe^{II}(DPAH)_2$ by PhNHNHPh, H_2NNH_2, $PhCH_2SH$, and H_2S.

A related binuclear complex,[18] $[(Ph_3PO)_4FeOOFe(OPPh_3)_4](ClO_4)_4$, also selectively dioxygenates PhC≡CPh and ketonizes methylene carbons.[12] With $(PA)_2FeOFe(PA)_2$·HOOH (**2**) the presence of substrate appears to be necessary to induce formation of the reactive intermediate complex [**3**(PhC≡CPh)].

Acknowledgment. This work was supported by the National Science Foundation under Grant No. CHE-8516247 (D.T.S.) and with a Graduate Fellowship (S.A.R.). We are grateful (a) to the U.S. Air Force Institute of Technology Civilian Institute Program for the award of a Fellowship to S.A.R. and (b) to the Universidad Catolicade Chile for a Research Leave to P.C.

(17) Cofré, P.; Sawyer, D. T. *Inorg. Chem.* **1986**, *25*, 2089-2092.

(18) Sawyer, D. T.; McDowell, M. S.; Spencer, L.; Tsang, P. K. S. *Inorg. Chem.* **1989**, *28*, 1166.

Contribution from the Department of Chemistry, The Pennsylvania State University, University Park, Pennsylvania 16802, and The Contrast Media Research Department, Squibb Institute for Medical Research, P.O. Box 191, New Brunswick, New Jersey 08903

Laser-Induced Europium(III) Luminescence and NMR Spectroscopic Characterization of Macrocyclic Diaza Crown Ether Complexes Containing Carboxylate Ligating Groups

Richard C. Holz,† Scott L. Klakamp,† C. Allen Chang,‡ and William DeW. Horrocks, Jr.*,†

Received October 3, 1989

The Eu^{3+} and Y^{3+} complexes of 1,10-diaza-4,7,13,16-tetraoxacyclooctadecane-*N*,*N*′-diacetic acid (K22DA), 1,7-diaza-4,10,13-trioxacyclopentadecane-*N*,*N*′-diacetic acid (K21DA), and the open-chain analogue ethylene glycol bis(β-aminoethyl ether)-*N*,*N*,*N*′,*N*′-tetraacetic acid (EGTA) have been characterized in solution by using Eu^{3+} laser-induced luminescence and ^1H and ^{13}C NMR spectroscopy. All of these ligands form 1:1 complexes with Eu^{3+} in solution with the luminescence lifetimes in H_2O and D_2O providing the number of coordinated water molecules. Stepwise changes in the coordination environment of the Eu^{3+} and Y^{3+} ions were monitored spectroscopically for each complex as a function of temperature. In addition, the Eu^{3+} spectral changes as a function of pH were examined. These results indicate that Eu^{3+} and Y^{3+} each coordinate all the ligating atoms of K21DA but that K22DA undergoes fluctional processes, suggesting that the macrocyclic cavity size is too large to accommodate the metal ion properly. The noncyclic EGTA ligand, by comparison, appears to undergo an equilibrium process of wrapping and unwrapping at room temperature. The luminescence and NMR results demonstrate the importance of a proper match between metal ion size and macrocyclic cavity size.

Introduction

Metal complexation by mixed aza and oxa macrocyclic ligands with or without coordinating pendant arms has recently received considerable attention. If certain features are "built" into these macrocyclic ligands, such as ligand charge density and/or macrocyclic cavity size, they can be designed to accommodate specific metal ions or groups of metal ions.[1,2] These macrocyclic ligands have many potential uses including synthetic ionophores, models of protein metal binding sites, NMR imaging agents, sequestering agents, and metal ion separation reagents. Specifically, we are interested in two macrocyclic aminocarboxylic acids that have binding selectivity toward the lanthanide ions in general and, within this series, toward individual lanthanide ions.[3-5] These two ligands, 1,10-diaza-4,7,13,16-tetraoxacyclooctadecane-*N*,*N*′-diacetic acid

†The Pennsylvania State University.
‡Squibb Institute for Medical Research.

(1) Lehn, J.-M. *Acc. Chem. Res.* **1978**, *11*, 49.
(2) Christensen, J. J.; Eatough, D. J.; Izatt, R. M. *Chem. Rev.* **1974**, *74*, 351.
(3) Chang, C. A.; Rowland, M. E. *Inorg. Chem.* **1983**, *22*, 3866.
(4) Chang, C. A.; Ochaya, V. O.; Sekhar, V. C. *J. Chem. Soc., Chem. Commun.* **1985**, 1724.
(5) Chang, C. A.; Ochaya, V. O. *Inorg. Chem.* **1986**, *25*, 355.

0020-1669/90/1329-2651$02.50/0

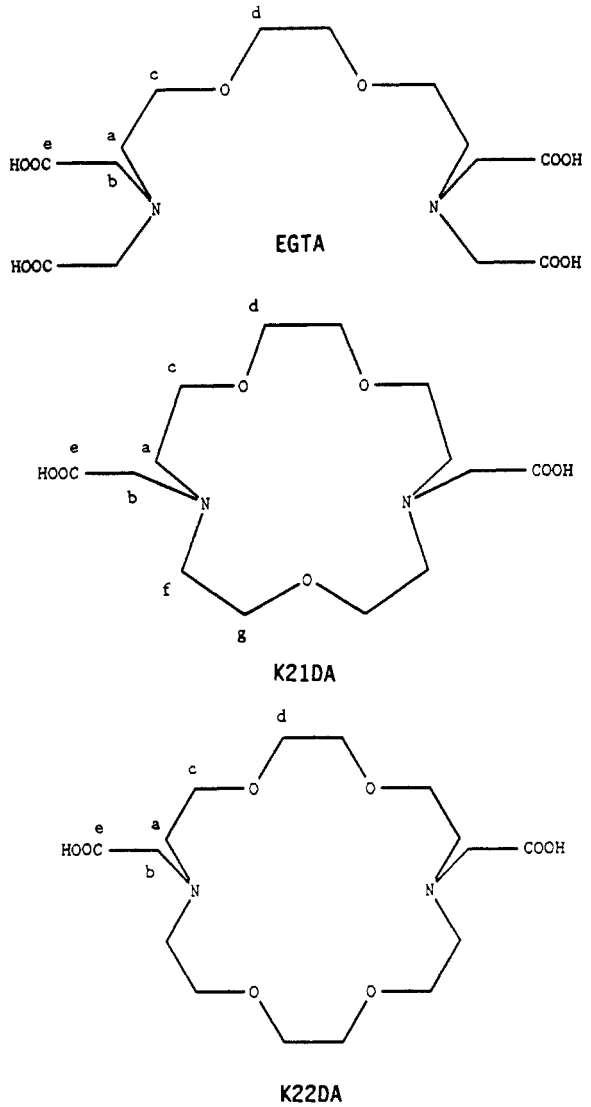

Figure 1. Schematics of the free ligands EGTA, K21DA, and K22DA with proton and carbon labels corresponding to those assigned to NMR chemical shifts in Tables III and IV.

(K22DA) and 1,7-diaza-4,10,13-trioxacyclopentadecane-*N,N'*-diacetic acid (K21DA), are shown in Figure 1 along with the open-chain analogue ethylene glycol bis(β-aminoethyl ether)-*N,N,N',N'*-tetraacetic acid (EGTA) for comparison purposes. Binding constants for K21DA with the lanthanide ion series reach a maximum at Eu^{3+} while those for K22DA are largest for Ce^{3+}.[5] In addition, both K21DA and K22DA have been shown to possess selectivity for a few transition-metal and post-transition-metal ions such as Cu^{2+}, Pb^{2+}, and Cd^{2+}.[6] The lanthanide complexes of K22DA and K21DA are reported to have unusual thermodynamic and kinetic properties but little is known about their structures in solution.[7-9]

Rare-earth ions have been used extensively in this laboratory to probe Ca^{2+} ion binding sites in proteins and to obtain structural information in solution on other biologically relevant systems.[10-12] The ability of Eu^{3+} and Tb^{3+} to luminesce in solution at room temperature makes them particularly appealing as structural probes.[12,13] The Eu^{3+} ion possesses nondegenerate ground ($^7F_0$) and first excited ($^5D_0$) states, neither of which can be split by the ligand field. The resulting transition consists of a single band for each distinct Eu^{3+} environment where the intensity is proportional to the metal complex concentration. The remaining energy levels of Eu^{3+} (e.g. $^5D_1$, $^5D_2$, etc.) are degenerate and will be split into the various Stark components of the ligand field, depending on the symmetry about the metal ion.

The $^7F_0 \rightarrow {}^5D_0$ excitation profile of Eu^{3+}, which appears in the 577–581-nm range, is obtained by scanning a tunable dye laser through the transition region while monitoring the "hypersensitive" $^5D_0 \rightarrow {}^7F_2$ emission band at 614 nm.[14] The present study explores the structural characteristics, in solution, of the Eu^{3+} and Y^{3+} complexes of K22DA and K21DA, as well as EGTA for comparison purposes. The Eu^{3+} complexes were studied by exploiting laser-induced luminescence and lifetime spectroscopic techniques, while the Y^{3+} complexes were probed by using ^1H and ^{13}C NMR spectroscopy.

Experimental Section

Materials. EGTA (98%) was purchased from the Sigma Chemical Co. Hydrated $EuCl_3$ (99.9%) and D_2O (99.8%) were purchased from the Aldrich Chemical Co. A 0.1 M $EuCl_3$ stock solution was prepared and standardized with EDTA by using an arsenazo indicator.[15] Rhodamine 590, Coumarin 485, and Coumarin 480 laser dyes were purchased from Exciton Co. while Rhodamine 610 was obtained from the Kodak Co. The H_2O used was doubly distilled while all remaining reagents were the purest commercially available. The ligands K22DA and K21DA were synthesized by the method of Kulstad and Malmsten with minor modifications as previously reported.[3,16]

Methods. The excitation and lifetime experiments were carried out using a Quantel series YG581C pulsed (10-Hz) Nd:YAG laser-pumped tunable dye laser Model TDL50 (~70 mJ/pulse). The remainder of the system was identical with that previously described.[17] A 10 mM stock solution (15 mM piperazine buffer, pH 6) was prepared for each ligand studied. Metal–ligand solutions used were typically prepared in a 1:1 ratio at a concentration of 10 μM, pH 6, unless otherwise stated. The $^7F_0 \rightarrow {}^5D_0$ transition (580 nm) of Eu^{3+} was excited by using a mixture of Rhodamine 590 and 610 dyes, the $^7F_0 \rightarrow {}^5D_1$ transition (525 nm) was excited by using Coumarin 485 dye, and the $^7F_0 \rightarrow {}^5D_2$ transition (465 nm) was accessed with Coumarin 480 dye. The laser line width (fwhm) is <0.02 nm at 580 nm. The $^5D_0 \rightarrow {}^7F_2$ emission band at 614 nm was monitored in each case. Emission spectra were recorded by directly exciting the $^5D_0$ level in the 580-nm region while scanning a Jobin-Yvon DH-20, 0.2-m double monochromator equipped with a microprocessor scan control unit. Entrance, intermediate, and exit slit widths of 0.5, 1.0, and 0.5 mm, respectively, were used, giving a bandpass of 1.5 nm.

^1H and ^{13}C NMR spectra were recorded on a Bruker AM-300 spectrometer at 300 and 75 MHz, respectively. A two-dimensional ^{13}C–^1H correlation spectrum (hetero-COSY) was also obtained on the same instrument. The ^1H and ^{13}C chemical shifts are reported relative to TMS as an external standard. NMR samples of K21DA, K22DA, and EGTA were prepared in a 1:1 metal–ligand ratio (D_2O, pH 6.0) at concentrations of 20, 20, and 100 mM, respectively. ^1H NMR ppm (Me_4Si, δ 0): EGTA, (a) 3.59 (t, 4), (b) 3.71 (s, 8), (c) 3.83 (s, 4), (d) 3.88 (t, 4); K21DA, (a) 3.56 (m, 8), (b) 3.71 (s, 4), (c) 3.85 (m, 4), (d), 3.88 (s, 4); K22DA, (a) 3.57 (s, 8), (c) 3.72 (s, 8), (b) 3,86 (s, 4), (d) 3.88 (s, 8). ^{13}C NMR ppm (Me_4Si, δ 0): EGTA, (a) 54.92, (b) 57.60, (c) 64.98, (d) 70.13, (e) 170.58; K21DA, (f) 53.34, (a) 55.22, (b) 55.93, (g) 63.11, (c) 63.44, (d) 69.95, (e) 169.82; K22DA, (a) 54.52, (b) 56.28, (c) 64.10, (d) 69.96, (e) 169.89. NMR probe temperatures were allowed to equilibrate for 15 min with the sample tube in the probe at each temperature before data acquisition. Reported temperature values are estimated to be accurate to ±1.0 °C.

Results and Discussion

Luminescence Characterization. The stoichiometries of the Eu^{3+} complexes of K21DA, K22DA, and EGTA were determined by titrating each ligand into a 10 μM $EuCl_3$ solution buffered at pH

(6) Delgado, R.; Da Silva, J. J. R. F.; Vaz, M. C. T. A. *Polyhedron* **1987**, *6*, 29.
(7) Sekhar, V. C.; Chang, C. A. *Inorg. Chem.* **1986**, *25*, 2061.
(8) Chang, C. A. Sekhar, V. C. *Inorg. Chem.* **1987**, *26*, 1981.
(9) Delgado, R.; da Silva, J. J. R. F.; Vaz, M. C. T. A.; Paoletti, P.; Micheloni, M. *J. Chem. Soc., Dalton Trans.* **1989**, 133.
(10) Horrocks, W. D., Jr.; Sudnick, D. R. *Acc. Chem. Res.* **1981**, *14*, 384.
(11) Horrocks, W. D., Jr.; Tingey, J. M. *Biochemistry* **1988**, *27*, 413.
(12) Horrocks, W. D., Jr.; Albin, M. *Prog. Inorg. Chem.* **1984**, *31*, 1.
(13) Reuben, J. *Bioinorganic Chemistry: Lanthanides as Probes in Systems of Biological Interest; Handbook on the Physics and Chemistry of Rare Earths*; Gschneidner, K. A., Eyring, L., Eds.; North-Holland: Amsterdam, 1979; Vol. 3, p 515.
(14) Albin, M. Ph.D. Thesis, The Pennsylvania State University, 1984.
(15) Fritz, J. S.; Oliver, R. T.; Pietrzyk, D. J. *Anal. Chem.* **1958**, *30*, 1111.
(16) Kulstad, S.; Malmsten, L. A. *Acta. Chem. Scand., Ser. B* **1979**, *B33*, 469.
(17) Holz, R. C.; Snyder, A. P.; Horrocks, W. D., Jr. *Lanthanide Actinide Res.* **1988**, *2*, 363.

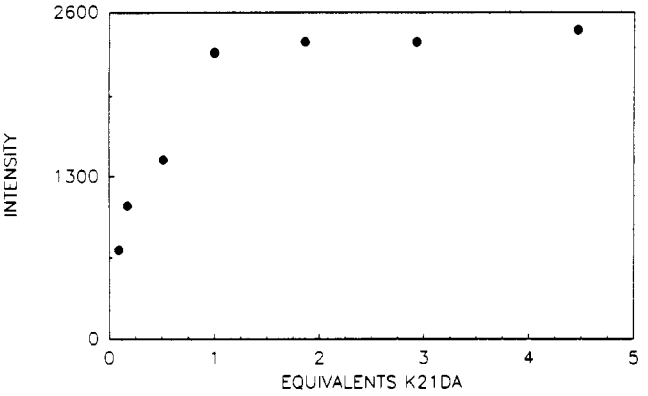

Figure 2. Photon flux (intensity) from the $^7F_0 \rightarrow {}^5D_0$ excitation of $[EuK21DA]^+$ (λ_{ex} = 579.7 nm, λ_{em} = 614 nm) as a function of equivalents of added K21DA.

Table I. $^7F_0 \rightarrow {}^5D_0$ Luminescence Results for the Eu^{3+} Complexes of K21DA, K22DA, and EGTA at 20 °C and pH 6.0

	λ,[a] nm	E, cm^{-1}	τ_H^{-1}, ms^{-1}	τ_D^{-1}, ms^{-1}	q[b]
		$[EuK21DA]^+$			
$^7F_0 \rightarrow {}^5D_0$	579.73	17249	2.70	0.67	2.1
		$[EuK22DA]^+$			
$^7F_0 \rightarrow {}^5D_0$	579.24	17264	2.17	0.84	1.4
	579.79	17248	2.17	0.84	1.4
	579.97	17242	2.17	0.84	1.4
		$[EuEGTA]^-$			
$^7F_0 \rightarrow {}^5D_0$	579.92	17244	1.75	0.49	1.3
	580.12	17238	1.75	0.49	1.3

[a] The reported wavelength values are accurate to ±0.02 nm. [b] Number of coordinated water molecules.

6 and plotting the photon flux resulting from $^7F_0 \rightarrow {}^5D_0$ excitation vs the equivalents of added ligand. All three of these ligands form 1:1 metal–ligand complexes as is illustrated by a typical titration curve of K21DA in Figure 2. The $^7F_0 \rightarrow {}^5D_0$ excitation spectrum of $[EuK21DA]^+$ consists of a single band, while the spectra of the remaining two complexes, $[EuEGTA]^-$ and $[EuK22DA]^+$, consist of two and three bands, respectively (Table I). All spectra were deconvoluted by using a Marquardt nonlinear regression algorithm employing a Lorentzian–Gaussian line-shape function.[18] The deconvoluted $^7F_0 \rightarrow {}^5D_0$ excitation spectrum of $[EuEGTA]^-$ is shown in Figure 3.

Luminescence decay curves, obtained separately in H_2O and D_2O, all consisted of only a single exponential at each wavelength tested across the spectral profile for each Eu^{3+} complex (Table I). Since only a single experimental decay curve is observed for $[EuK22DA]^+$ and $[EuEGTA]^-$, the multiple species detected in the excitation spectra are necessarily in fast exchange on the $^5D_0$ excited-state time scale.[19] Horrocks and Sudnick[20] have previously reported a method that allows the determination of the number of coordinated water molecules. This method involves the replacement of H_2O by D_2O, which essentially eliminates the vibronic deexcitation pathway provided by the OH oscillators of bound water molecules. The relationship between the number of coordinated water molecules, q, and the reciprocal excited-state lifetimes is

$$q = 1.05(\tau_{H_2O}^{-1} - \tau_{D_2O}^{-1}) \quad (1)$$

The lifetime data obtained for $[EuEGTA]^-$, $[EuK22DA]^+$, and $[EuK21DA]^+$ reveal that these complexes contain 1.3, 1.4, and 2.1 coordinated water molecules, respectively (Table I). The fractional values obtained for the first two species may represent weighted averages of complexes with one and two coordinated water molecules since more than one complex is present, as evidenced by the excitation spectra.

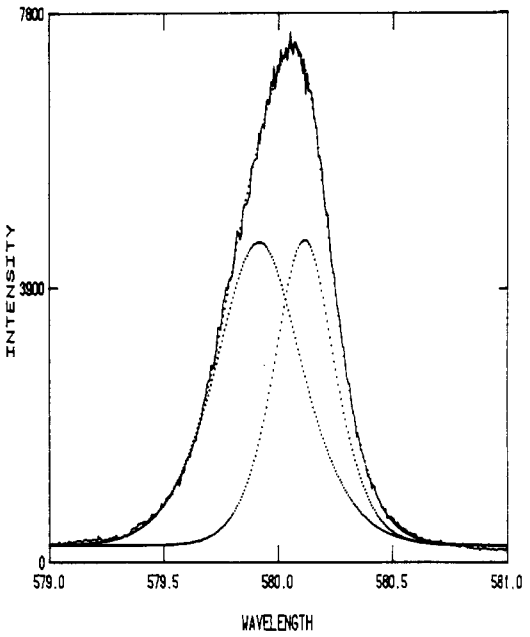

Figure 3. Curve-resolved $^7F_0 \rightarrow {}^5D_0$ excitation spectrum of $[EuEGTA]^-$ at pH 6.0 obtained by using Lorentzian–Gaussian type peaks.

Table II. Ligand Field Splitting of the $^5D_1$ and $^5D_2$ Levels of Eu^{3+}–K21DA, –K22DA, and –EGTA at 20 °C and pH 6.0

	λ,[a] nm	E, cm^{-1}		λ,[a] nm	E, cm^{-1}
		$[EuK21DA]^+$			
$^7F_0 \rightarrow {}^5D_1$	525.34	19035	$^7F_0 \rightarrow {}^5D_2$	464.86	21512
	525.80	19019		465.06	21503
	526.25	19002		465.54	21480
				466.04	21457
		$[EuEGTA]^-$			
$^7F_0 \rightarrow {}^5D_1$	525.24	19034	$^7F_0 \rightarrow {}^5D_2$	465.19	21497
	526.08	19009		465.89	21464
	526.38	18998		466.18	21451
		$[EuK22DA]^+$			
$^7F_0 \rightarrow {}^5D_1$	525.23	19039	$^7F_0 \rightarrow {}^5D_2$	464.98	21506
	525.70	19022		465.37	21488
	525.94	19014		465.69	21474
	526.74	18985		466.25	21448
				466.45	21439

[a] The reported wavelength values are accurate to ±0.02 nm.

Excitation from the ground state of Eu^{3+} to other higher energy excited states (e.g. $^7F_0 \rightarrow {}^5D_1$ and $^7F_0 \rightarrow {}^5D_2$ transitions) were recorded for each complex in order to determine the ligand-field splitting of the Eu^{3+} $^5D_1$ and $^5D_2$ energy levels (Table II). The number of transitions observed in these spectra provides an indication of the symmetry about the Eu^{3+} ion.[21] For $[EuK21DA]^+$, four bands appear in the $^7F_0 \rightarrow {}^5D_2$ spectrum, three bands in the $^7F_0 \rightarrow {}^5D_1$ spectrum, and one in the $^7F_0 \rightarrow {}^5D_0$ spectrum. These data indicate a Eu^{3+} site symmetry of C_{2v} or less for $[EuK21DA]^+$. For $[EuK22DA]^+$ and $[EuEGTA]^-$, the unambiguous assignment of metal ion site symmetry is not possible due to the multiple species present in solution for both complexes. However, the symmetry is likely to be low, probably less than C_{2v}. The emission spectrum of each complex was also recorded while the $^7F_0 \rightarrow {}^5D_0$ transition was being excited. Due to the limited emission spectral resolution, no differences in spectra were observed for $[EuK22DA]^+$ and $[EuEGTA]^-$, even with preferential excitation of each $^7F_0 \rightarrow {}^5D_0$ transition.

(18) McNemar, C. W.; Horrocks, W. D., Jr. *Appl. Spectrosc.* **1989**, *43*, 816.
(19) Horrocks, W. D., Jr.; Arkle, V. K.; Liotta, F. J.; Sudnick, D. R. *J. Am. Chem. Soc.* **1983**, *105*, 3455.
(20) Horrocks, W. D., Jr.; Sudnick, D. R. *J. Am. Chem. Soc.* **1979**, *101*, 334.
(21) Thompson, L. C. *Complexes, Handbook on the Physics and Chemistry of Rare Earths*, Gschneidner, K. A., Eyring, L., Eds.; North-Holland: Amsterdam, 1979; pp 211–2.

The luminescence results presented thus far indicate that all three ligands coordinate one metal ion; the resulting complexes of EGTA and K22DA coordinate on average just slightly more than one water molecule, while the K21DA complex coordinates two. The difference in the number of bound water molecules for the K22DA and K21DA complexes can be attributed to the extra ether oxygen in the macrocyclic ring of K22DA, which appears to coordinate directly to the metal ion. EGTA, on the other hand, permits coordination of only a single water molecule. Assuming that coordination of all potential ligating atoms occurs, our data suggest coordination numbers of 9 for each complex, a value that is reasonable for rare-earth-metal ions.[22] The multiple species observed for EGTA and K22DA, but not K21DA, may be attributed to the macrocyclic cavity size of K22DA and the noncyclic character of EGTA, as well as the increased number of coordinating carboxylic acid arms in EGTA.

The cavity sizes of K21DA and K22DA are approximately the same as in the well-known macrocyclic ethers 15-crown-5 and 18-crown-6, respectively. The diameters of the macrocyclic cavities range from 2.1 to 2.8 Å, which are in good agreement with Eu^{3+} ion diameters (2.1–2.5 Å), depending on coordination number.[23] The Eu^{3+} diameter is better suited for 15-crown-5 than 18-crown-6, implying that K21DA, rather than K22DA, should more effectively accommodate Eu^{3+}. Furthermore, the pendant carboxylate arms of K21DA and K22DA increase the ligand binding ability by holding the metal ion more securely in the macrocyclic cavity. The use of charged pendant moieties allows a particular macrocycle to be "tuned" to fit the metal ion of choice by combining the correct ligand charge density with the proper macrocyclic cavity size. In the cases of K21DA and K22DA, the former appears to supply the more optimal binding properties for Eu^{3+}.

The importance of cavity size is additionally reflected in the stability constants of the Eu^{3+} complexes of K21DA and K22DA, particularly when they are compared with those of the remaining lanthanide ions.[5] Of all the lanthanide ions, Eu^{3+} forms the most stable complex with K21DA, indicating a "correct fit" of the macrocycle to Eu^{3+}. The larger Ce^{3+} ion, on the other hand, forms the most stable complex with K22DA, demonstrating the importance of a match between the macrocyclic cavity size and the metal ion diameter. The imperfect fit of Eu^{3+} within the macrocyclic cavity of K22DA is a possible cause of the multiple species present in solution. By comparison, EGTA is noncyclic with four liganding carboxylate groups and has the ability to "wrap" around the metal ion; this gives it increased stability, but little selectivity. In order to gain further insight into the nature of the multiple species present for $[EuK22DA]^+$ and $[EuEGTA]^-$, the $^7F_0 \rightarrow {}^5D_0$ spectrum of each complex was monitored as a function of pH and temperature.

As the pH is systematically increased from 2 to 10, neither the $^7F_0 \rightarrow {}^5D_0$ spectrum nor the excited-stated lifetime of $[EuEGTA]^-$ changes. However, spectral and lifetime changes were observed for both of the macrocyclic complexes. The $^7F_0 \rightarrow {}^5D_0$ excitation peak of $[EuK21DA]^+$ centered at 579.73 nm decreases in intensity as the pH is raised above 7.0, with the concomitant appearance of a new band centered at 579.85 nm. The excited-state lifetime of the species corresponding to this new band is 730 μs at pH 10, an increase of 360 μs; this corresponds to the monodeprotonation of each of the two water molecules or the complete loss of a single water molecule. As the pH is increased above pH 7.0, the three bands of $[EuK22DA]^+$ (Table I and Figure 4) decrease in intensity, with the simultaneous appearance of two new bands centered at 578.49 and 578.93 nm. Above pH 9.5, the original bands are no longer observable (Figure 4). The new bands both exhibit the same lifetime of 675 μs, an increase of 205 μs over the neutral pH value, corresponding to the monodeprotonation of a single water molecule. The shift of the $^7F_0 \rightarrow {}^5D_0$ transition of $[EuK21DA]^+$ to higher wavelength as a function of increasing pH is expected for additional negatively charged species in contact with the metal center.[24] However, the two new bands appearing

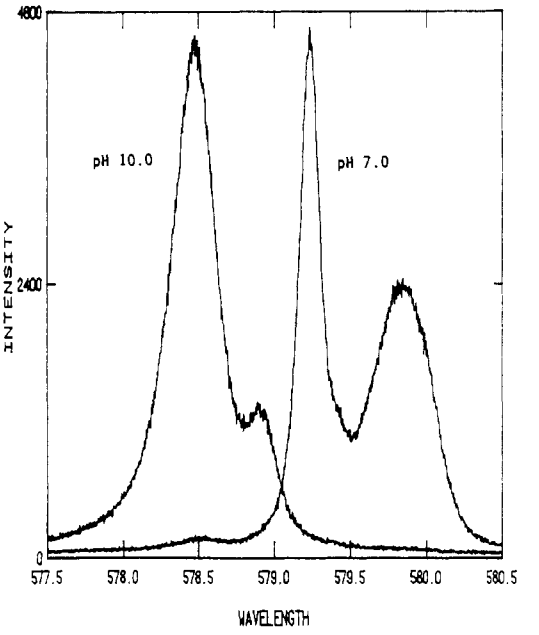

Figure 4. $^7F_0 \rightarrow {}^5D_0$ excitation spectrum of Eu^{3+} bound to K22DA at pH values of 7.0 and 10.0 and 20 °C.

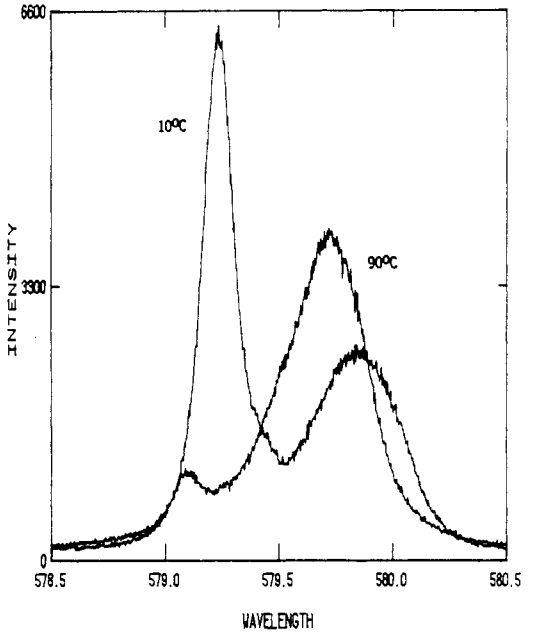

Figure 5. $^7F_0 \rightarrow {}^5D_0$ excitation spectrum of Eu^{3+} bound to K22DA at 10 and 90 °C and pH 6.0.

at shorter wavelength in the $^7F_0 \rightarrow {}^5D_0$ spectrum of $[EuK22DA]^+$ appear also to be due to the mondeprotonation of a single water molecule, suggesting that a variety of factors may contribute to the determination of the excitation wavelength. Similar appearances of shorter wavelength excitation bands at higher pH values have been reported by Henzl and Birnbaum[25] and by McNemar and Horrocks[26] for Eu^{3+}-loaded samples of several parvalbumins. This pH phenomenon is currently under further investigation.

The $^7F_0 \rightarrow {}^5D_0$ excitation band of each metal–ligand complex was additionally monitored as a function of temperature at pH 6.0. The $[EuK21DA]^+$ and $[EuEGTA]^-$ spectral and excited-state lifetime data remain unaltered as the temperature is increased

(22) Sinha, S. P. *Struct. Bonding (Berlin)* **1976**, *25*, 69.
(23) Bunzli, J.-C. G.; Wessner, D. *Isr. J. Chem.* **1984**, *24*, 313.
(24) Albin, M.; Horrocks, W. D., Jr. *Inorg. Chem.* **1985**, *24*, 895.
(25) Henzl, M. T.; Birnbaum, E. R. *J. Biol. Chem.* **1988**, *263*, 10674.
(26) McNemar, C. W.; Horrocks, W. D., Jr. *Biochim. Biophys. Acta*, in press.

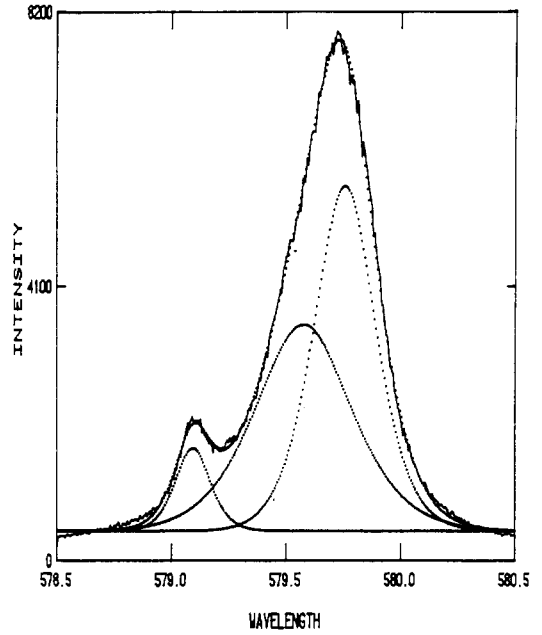

Figure 6. Curve-resolved Eu^{3+} $^7F_0 \rightarrow {}^5D_0$ excitation spectrum of $[EuK22DA]^+$ at 90 °C and pH 6.0 obtained by using Lorentzian–Gaussian type peaks.

from 15 to 96 °C. However, for $[EuK22DA]^+$, these properties exhibit a significant temperature dependence (Figure 5). The $^7F_0 \rightarrow {}^5D_0$ spectrum of $[EuK22DA]^+$ at high temperature is resolvable into three bands (Figure 6). The band centered at 579.09 nm becomes nearly undetectable, while the bands centered at 579.58 and 579.76 nm increase in intensity with increasing temperature. The excited-state lifetime of $[EuK22DA]^+$, recorded at several wavelengths across the peak profile, remains unchanged at all temperatures. The nature of the equilibrium process responsible for these observations is not known, but may be attributed to fluctional processes involving the acetate groups or the ether oxygens of the macrocyclic ring. The single species responsible for the excitation band at 579.09 nm appears to be in equilibrium with the two species that produce the broad, but resolvable, asymmetric band centered at 579.69 nm. The spectral differences between $[EuK21DA]^+$ and $[EuK22DA]^+$ likely originate in the size and binding characteristics of the macrocyclic ring; these characteristics were further explored by ^1H and ^{13}C NMR spectroscopy.

NMR Characterization. Y^{3+} was chosen as a diamagnetic replacement for Eu^{3+} over La^{3+} or Lu^{3+} because its ionic radius and chemical properties are more similar to those of Eu^{3+}. ^1H and ^{13}C NMR spectra were recorded for the Y^{3+} complexes at various temperatures from 275 to 354 K. Selected NMR data are reported in Tables III and IV, with assignments referred to the labeling schemes shown in Figure 1. A partial proton NMR spectrum of $[YEGTA]^-$ has been previously reported[27] and is in full agreement with our results.

Day and Reilley reported[28,29] a method of qualitatively determining bond labilities of ligands from specific ^1H splitting patterns. Four different splitting patterns were observed for metal complexes of EDTA. The simplest pattern contains two singlets, indicating short-lived metal–nitrogen and metal–oxygen bonds. The second splitting pattern consists of an AB quartet for the acetate protons and a singlet for the ethylenic protons; this indicates short-lived metal–oxygen and long-lived metal–nitrogen bonds, the latter preventing inversion through the nitrogens. The third case is the most complicated, with multiplets being observed for both the acetate and ethylenic protons due to long-lived metal–nitrogen and metal–oxygen bonds. The final case involves long-lived metal–oxygen and short-lived metal–nitrogen bonds and is indistinguishable experimentally from the second case. The acetate proton splitting patterns of the Y^{3+} complexes of EGTA, K22DA, and K21DA are expected to fall into one of these four categories.

The ^1H NMR spectrum of $[YEGTA]^-$ at 300 MHz, 20 °C, contains a broad singlet for the acetate protons (b), similar to that previously reported in the 60-MHz spectrum.[28] The remainder of the spectrum contains a broad downfield singlet (d) that overlaps a broadened multiplet (c) and two broad upfield singlets (a) (Table III). These data suggest short-lived metal–acetate oxygen and intermediate-lived metal–nitrogen bonds, since the acetate resonance is exchange broadened. The proton-decoupled ^{13}C NMR

Table III. Selected ^1H NMR Chemical Shift Data (ppm) for $[YK21DA]^+$ and $[YEGTA]^-$ at Various Temperatures and pH 6.0

275 K	$[YEGTA]^-$	(a) NCH_2CH_2	2.55 (d, 2, J = 12 Hz)
		(a) NCH_2CH_2	2.94 (t, 2, J = 10 Hz)
		(b) NCH_2COOH	3.20, 3.28 (d, 8, J = 24 Hz)
	$[YK21DA]^+$	(a or g) NCH_2CH_2	2.58 (t, 4, J = 9 Hz)
		(a or g) NCH_2CH_2	2.90 (m, 4)
		(b) NCH_2COOH	3.12, 3.18, 3.25, 3.30 (AB, 4)
293 K	$[YEGTA]^-$	(a) NCH_2CH_2	3.14; 2.78 (s, 2; s, 2)
		(b) NCH_2COOH	3.44 (s, 8)
	$[YK21DA]^+$	(a and g) NCH_2CH_2	2.79; 3.11 (m, 4; m, 4)
		(b) NCH_2COOH	3.34, 3.39, 3.46, 3.52 (AB, 4)
303 K	$[YEGTA]^-$	(a) NCH_2CH_2	...
		(b) NCH_2COOH	3.56 (s, 8)
	$[YK21DA]^+$	(a and g) NCH_2CH_2	2.88; 3.20 (m, 4; m, 4)
		(b) NCH_2COOH	3.42, 3.48, 3.55, 3.61 (AB, 4)
327 K	$[YEGTA]^-$	(a) NCH_2CH_2	3.31 (s, 4)
		(b) NCH_2COOH	3.79 (s, 8)
	$[YK21DA]^+$	(a and g) NCH_2CH_2	3.07; 3.41 (m, 4; m, 4)
		(b) NCH_2COOH	3.62, 3.67, 3.75, 3.80 (AB, 4)
354 K	$[YK21DA]^+$	(a and g) NCH_2CH_2	3.46; 3.77 (m, 4; m, 4)
		(b) NCH_2COOH	3.99, 4.05, 4.13, 4.18 (AB, 4)

Table IV. ^{13}C NMR Chemical Shift Data (ppm) for $[YK21DA]^+$, $[YK22DA]^+$, and $[YEGTA]^-$ at Various Temperatures and pH 6.0

		$[YEGTA]^-$	$[YK21DA]^+$	$[YK22DA]^+$
275 K	(a) NCH_2CH_2O	57.56	53.52	54.39, 56.81
	(b) NCH_2COOH	61.93, 63.78	62.93	62.90
	(c) NCH_2CH_2O	70.00	69.05	68.45, 69.92
	(d) OCH_2CH_2O	70.82	70.26	70.47, 70.71
	(e) NCH_2COO^-	180.09, 180.25	179.62	179.76
	(f) NCH_2CH_2O		54.21	
	(g) NCH_2CH_2O		69.59	
293 K	(a) NCH_2CH_2O	57.76	53.75	54.62, 57.05
	(b) NCH_2COOH	62.27, 63.99	63.12	63.25
	(c) NCH_2CH_2O	70.21	69.32	68.75, 70.24
	(d) OCH_2CH_2O	71.00	70.49	70.89
	(e) NCH_2COO^-	180.31	179.84	179.92
	(f) NCH_2CH_2O		54.42	
	(g) NCH_2CH_2O		69.89	
303 K	(a) NCH_2CH_2O	57.90	53.87	54.67, 57.04
	(b) NCH_2COOH	...	63.22	63.35
	(c) NCH_2CH_2O	70.34	69.46	68.86, 70.09
	(d) OCH_2CH_2O	71.11	70.61	70.98
	(e) NCH_2COO^-	180.37	179.91	180.14
	(f) NCH_2CH_2O		54.52	
	(g) NCH_2CH_2O		70.05	
327 K	(a) NCH_2CH_2O	58.16	54.08	...
	(b) NCH_2COOH	63.46	63.39	63.76
	(c) NCH_2CH_2O	70.59	69.71	...
	(d) OCH_2CH_2O	71.26	70.82	71.32
	(e) NCH_2COO^-	180.43	180.24	180.32
	(f) NCH_2CH_2O		54.70	
	(g) NCH_2CH_2O		70.30	
354 K	(a) NCH_2CH_2O		54.57	56.67
	(b) NCH_2COOH		64.09	64.12
	(c) NCH_2CH_2O		70.25	70.22
	(d) OCH_2CH_2O		71.32	71.63
	(e) NCH_2COO^-		180.64	180.72
	(f) NCH_2CH_2O		55.32	
	(g) NCH_2CH_2O		70.87	

(27) Mirti, P.; Gennaro, M. C. *J. Inorg. Nucl. Chem.* **1981**, *43*, 3221.
(28) Day, R. J.; Reilley, C. N. *Anal. Chem.* **1964**, *36*, 1073.
(29) Day, R. J.; Reilley, C. N. *Anal. Chem.* **1965**, *37*, 1326.

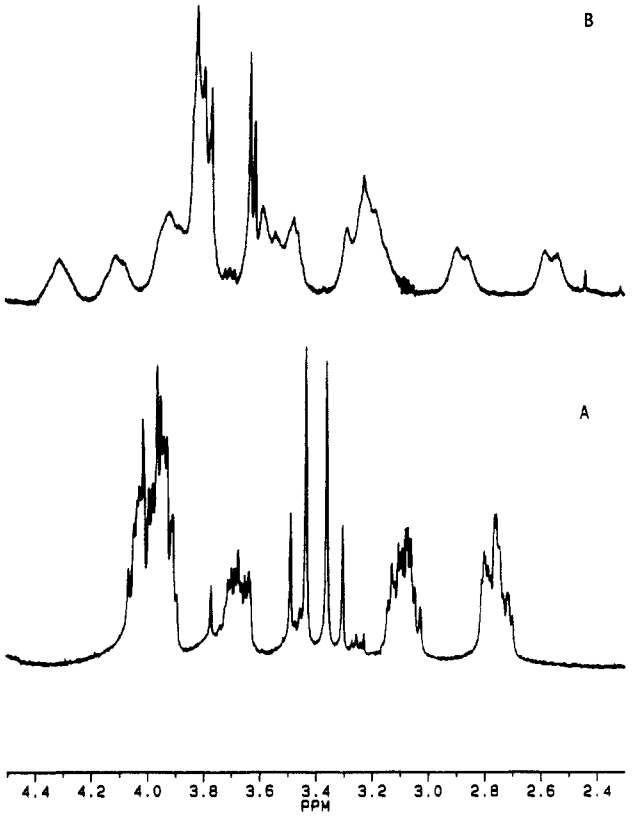

Figure 7. ^1H NMR spectra of (A) $[YK21DA]^+$ and (B) $[YK22DA]^+$ at 20 °C and pH 6.0.

spectrum of $[YEGTA]^-$ was recorded at 20 °C and contains six resonances, all of which are shifted downfield from the free ligand resonances, indicative of complete ligand binding. Of these six resonances, four are sharp, intense singlets while the remaining two are broad weak singlets. This broadening is likely due to a fluctional process which occurs at a rate slower than that of the NMR time scale.

In order to assign unambiguously the ^{13}C resonances of $[YEGTA]^-$, a ^{13}C–^1H correlated two-dimensional (hetero-COSY) experiment was performed. These data indicate that the two broadened carbon resonances at 62.27 and 63.99 ppm are coupled to the acetate protons (b), establishing them as the resonances due to the acetate carbons. This suggests that while the acetate protons interchange at a rate which is intermediate on the NMR time scale, the acetate carbons interconvert slowly. The resonance at 57.76 ppm is coupled to the two broadened proton singlets of the amino–ether ring, indicating that it is due to the ethylenic carbons (a) whose protons are in slow exchange on the NMR time scale. The remaining resonances at 71.00 and 70.21 ppm are coupled to the broad singlet and multiplet assigned to the protons adjacent to the ether oxygens; these have been assigned to the carbons adjacent to the ether oxygens (c and d).

The ^1H and ^{13}C NMR spectra of $[YK21DA]^+$ and $[YK22DA]^+$ were recorded at 20 °C, and spectral assignments were made by comparison of the results obtained from the $[YEGTA]^-$ correlated spectrum. The ^1H NMR spectrum of $[YK21DA]^+$ consists of four multiplets, two upfield from an AB quartet centered at 3.42 ppm due to the acetate protons (a) and two downfield (Figure 7A). The two upfield multiplets integrate in a 1:1 ratio and are probably due to the ethylenic protons nearest the amine nitrogens (a and f). The two downfield resonances integrate in a 2:1 ratio and are likely from the protons adjacent to the ether oxygens (c, d, and g). These resonances are excessively split due to proton coupling of the ethylenic bridges of the asymmetric macrocyclic ring. The observed AB pattern corresponds to the second limiting case involving long-lived metal–nitrogen and short-lived metal–acetate oxygen bonds. The proton-decoupled ^{13}C NMR spectrum contains six sharp resonances

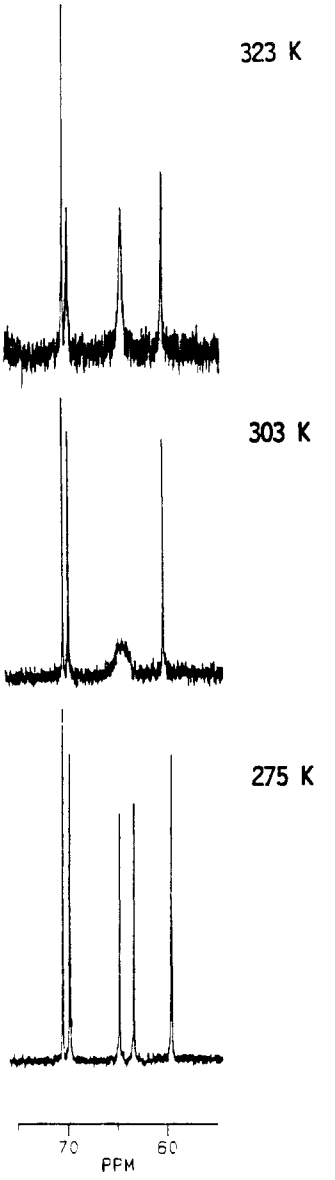

Figure 8. ^{13}C NMR spectra of $[YEGTA]^-$ as a function of temperature: (A) 275 K; (B) 303 K; (C) 323 K.

whose chemical shifts are consistent with coordination of all the ligating atoms. The ^1H NMR spectrum of $[YK22DA]^+$, conversely, is quite complicated due to proton coupling and fluctional processes that cause considerable broadening (Figure 7B). This spectrum consists of several poorly resolved multiplets yielding no useful structural data and therefore will not be discussed further. The proton-decoupled ^{13}C NMR spectrum of $[YK22DA]^+$ contains seven resonances, three of which are sharp singlets centered at 63.25, 70.89, and 179.92 ppm corresponding to the acetate carbons (b), the diether–ethylenic carbons (d), and the carboxylate carbons (e), respectively. The four remaining resonances are less intense and broadened, with chemical shifts of 54.67, 57.05, 68.75, and 70.24 ppm. The two upfield resonances are assigned to the carbons adjacent to the amine nitrogen (a) while the two downfield resonances are assigned to the carbons nearest the ether oxygens (c). These data indicate that a fluctional process occurs for these carbons in which the interconversion rates are slow to intermediate on the NMR time scale.

Spectra were obtained for each complex at several temperatures ranging from 3 to 81 °C (Tables III and IV). The broad acetate resonance in the ^1H NMR spectrum of $[YEGTA]^-$ at 20 °C splits into a doublet (25.52 Hz) at 3 °C. At this temperature the two broad upfield singlets (a) split into a broadened triplet and a doublet centered at 2.57 and 2.94 ppm, respectively. The exchange-broadened ^{13}C resonances of the acetate carbons (b) are

Table V. Kinetic and Activation Thermodynamic Parameters for Conformational Dynamics of the Y^{3+} Complexes of K22DA and EGTA[a]

	[YEGTA]$^-$	[YK22DA]$^+$ (a)[b]	[YK22DA]$^+$ (b)[b]
T_c, K	303	327	327
$\Delta\nu$, Hz	140.0	110.0	182.7
k_c, s^{-1}	310	240	410
$\Delta G^{\ddagger}_c$, kJ mol^{-1}	61.7	65.3	63.9

[a] Errors estimated for each value given are ±1 °C for T_c, ±0.5 Hz for $\Delta\nu$, ±20 s^{-1} for k_c, and ±10% for $\Delta G^{\ddagger}_c$. Actual systematic errors may potentially be much larger. [b] The a and b designations refer to the downfield and upfield coalescent ^{13}C resonances, respectively.

well-resolved (140.00 Hz) at 3 °C and are proportionally similar in intensity and full width at half-maximum (fwhm) to the other resonances in the spectrum (Figure 8). The coalescence temperature for these resonances was found to be 30 °C, which is identical with that of the upfield proton resonances. As the temperature is increased to 54 °C, the acetate resonance (b) becomes sharp, with the remainder of the spectrum containing three sharp singlets. The ^{13}C spectrum at temperatures above 30 °C contains five sharp singlets, the expected number if no intermediate or slow exchange processes are occurring.

The ^1H and ^{13}C NMR spectra of $[YK21DA]^+$ remain unchanged at all temperatures studied, while both the ^1H and ^{13}C NMR spectra of $[YK22DA]^+$ show a marked temperature dependence. It is apparent that several fluctional processes occur for the macrocyclic protons of $[YK22DA]^+$; however, the spectrum remains quite complicated at all temperatures, defying a definitive interpretation. On the other hand, the proton-decoupled ^{13}C NMR spectrum is quite informative from a structural standpoint. At 3 °C eight resonances are observed, rather than the original seven observed at room temperature. The extra resonance appears to be due to the slowing of a fluctional process involving the diether–ethylenic carbons (d). The decrease in temperature slows this interconversion enough to allow the observation of each carbon site. The remaining two exchange processes involving ethylenic carbons (a) and (c) are well resolved (110.00 Hz for the downfield resonances (a) and 182.70 Hz for the upfield resonances (b)). Both sets of resonances are very similar in intensity and fwhm relative to the other resonances in the spectrum. At 13 °C the diether–ethylenic carbons (d) exhibit a broadened resonance and at 54 °C the remaining resonances coalesce due to fluctional processes. As the temperature is increased further, five carbon resonances appear as if in a rapid exchange limit.

Rate constants and free energies of activation at the coalescence temperatures (T_c), for dynamic processes such as those described here, can be calculated from the frequency differences in the absence of exchange ($\Delta\nu$ in hertz).[30] These kinetic parameters, calculated by using eqs 2 and 3, are given in Table V. Exchange

$$k_c = \Delta\nu/2 \tag{2}$$

$$\Delta G^{\ddagger}_c = 2.3RT_c(10.319 + \log(T_c/k_c)) \tag{3}$$

rate constants were determined only for the fluctional processes observed for the acetate carbons (b) of $[YEGTA]^-$ and for the ethylenic carbons nearest the amine nitrogens (a) and ether oxygens (c) of $[YK22DA]^+$ (Table V). In order to calculate exchange rate constants, the difference in frequency between fluctional resonances in the absence of exchange is needed. While the differences reported here are those observed at the lowest working temperature, they may in fact not be the limiting values. Therefore, the rate constant values reported here are only lower limits for the rate constants for these exchange processes. The kinetic values determined for $[YEGTA]^-$ and $[YK22DA]^+$ are in good agreement with kinetic parameters reported for EDTA and DTPA complexes of rare-earth-metal ions.[31,32]

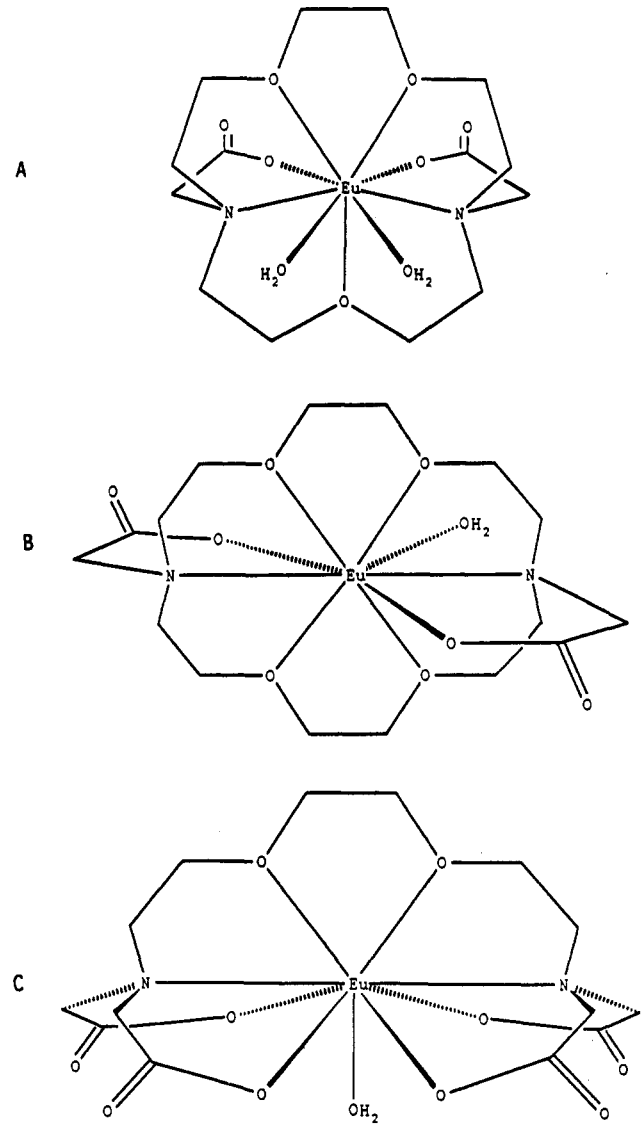

Figure 9. Schematics of the possible solution structures of the Eu^{3+} complexes of (A) K21DA, (B) K22DA, and (C) EGTA.

These NMR results reiterate the importance of the correlation of metal ion size with the macrocyclic cavity size. These data suggest that the Y^{3+} ion coordinates each ligating atom in the K21DA ring as well as the carboxylic acid oxygens at all temperatures. However, the K22DA macrocycle undergoes fluctional processes, indicating that the macrocyclic ring is too large to accommodate the metal ion properly. These fluctional processes suggest that some ether oxygen atoms of the K22DA macrocyclic ring may fluctuate between bound and unbound states. The noncyclic EGTA ligand, by comparison, appears to undergo an equilibrium process of wrapping and unwrapping at room temperature, as previously reported.[27] These processes are significantly slowed as the temperature is lowered.

Conclusion

The combination of Eu^{3+} luminescence and NMR spectroscopy provides a reasonably detailed analysis of the solution structures of the complexes studied here. From the luminescence data the metal–ligand stoichiometry and number of coordinated water molecules has been obtained, while the ^1H and ^{13}C NMR data describe bond labilities and fluctional processes that occur about the metal center. The results obtained regarding the complex formation of K21DA are the most straightforward; they indicate a 1:1 metal–ligand complex, complete coordination of all the macrocyclic ligating atoms, and two coordinated water molecules.

(30) Sandstrom, J. *Dynamic NMR Spectroscopy*; Academic Press: New York, 1982; pp 79–96.
(31) Gennaro, M. C.; Mirti, P.; Casalino, C. *Polyhedron* **1983**, *2*, 13.
(32) Jenkins, B. G.; Lauffer, R. B. *Inorg. Chem.* **1988**, *27*, 4730.

The resulting complex is nine-coordinate and possesses symmetry no higher than C_{2v} (Figure 9A). This structure exemplifies an appropriate match between a metal ion and the cavity size and charge density of a macrocyclic ligand.

Precise structural predictions about the remaining two metal-ligand complexes are more difficult to make, owing to the multiple species present in solution; however, a number of conclusions can be reached. The results for the binding of K22DA to Eu^{3+} indicate a 1:1 metal-ligand complex with one coordinated water molecule. This ligand, like EGTA, undergoes fluctional processes that result in incomplete binding of the macrocycle. These processes are temperature dependent, as marked changes are observed in the luminescence and NMR spectra with increasing temperature. The complex present at 20 °C appears to be a nine-coordinate species with all the ligating atoms of the macrocyclic ring and two carboxylate oxygens binding along with a single water molecule (Figure 9B). The fluctional processes observed for these ligand-metal complexes are indicative of a poor correlation between the macrocyclic cavity size and ligand charge density with regard to Eu^{3+} and Y^{3+} binding.

Finally, the complex formed by EGTA appears to be in an equilibrium process of wrapping and unwrapping, which places the Eu^{3+} ion in two distinct, but similar, chemical environments. However, these two species are in fast exchange on the Eu^{3+} luminescence ($^5D_0$) lifetime scale. This unwrapping process is also suggested by the NMR bond labilities, which demonstrate that the metal-nitrogen and metal-acetate oxygen bond lifetimes are short on the NMR time scale. These data suggest complete binding of each ligating atom of EGTA with an equilibrium process occurring, possibly between eight- and nine-coordinate species (Figure 9C).

The proposed structures of these complexes are in good agreement with the available X-ray crystallographic data. While no X-ray crystallographic data are available for the lanthanide complexes of these ligands, two relevant structures have recently been reported.[33,34] The first is the Ca^{2+} complex of EGTA.[33] These structural data indicate an eight-coordinate complex with all ligating atoms directly coordinating the Ca^{2+} ion. Three $[CaEGTA]^{2-}$ species exist in the crystal lattice with approximate dodecahedral geometry; however, they are bridged by Ca^{2+} counterions through the EGTA carboxylate arms, forming a polymeric structure. The inner coordination sphere of Ca^{2+} bound to EGTA is similar to the structure proposed here for the Eu^{3+} complex on the basis of NMR and luminescence data. The only difference between these structures is that the Eu^{3+} ion has extended its coordination number to nine by binding a water molecule. The second crystallographic study involves the structure of the Eu^{3+} complex of the 1,10-diaza-4,7,13,16-tetraoxacyclooctadecane macrocycle,[34] which contains no carboxylate groups. Three distinct metal complexes exist in the crystal lattice, one being $[Eu(NO_3)_6]^{3-}$. The remaining two species differ in the way in which the macrocycle coordinates the metal ion. The first species has C_2 symmetry with the Eu-N and Eu-O distances being very similar, while the second complex is best described as elliptical with the Eu-N bond distances being much longer than the Eu-O distances. These structures are in excellent agreement with the NMR and luminescence data, which suggest an uncomfortable fit of this macrocycle to Eu^{3+}. The multiple species present for the Eu^{3+} and Y^{3+} complexes may be due to an equilibrium process involving metal-nitrogen bond breakage and subsequent re-formation.

Acknowledgment. We gratefully acknowledge the financial support provided by the National Science Foundation (Grant CHEM-8821707). We thank Dr. Patrick J. Breen and Dr. Charles W. McNemar for writing portions of the computer software used in this research. We are also grateful to Dr. Alan J. Benesi for his invaluable technical support in the NMR experiments.

(33) Schauer, C. K.; Anderson, O. P. *J. Am. Chem. Soc.* **1987**, *109*, 3646.
(34) Nicolo, F.; Plancherel, D.; Chapuis, G.; Bunzli, J.-C. G. *Inorg. Chem.* **1988**, *27*, 3518.

Contribution from the Laboratory of Polymer Chemistry, University of Groningen, Nijenborg 16, 9747 AG Groningen, The Netherlands

Addition of Phosphazenocuprates to Aldehydes and Ketones: A New Route to *gem*-Organo-Substituted Cyclotriphosphazenes

Pieter L. Buwalda, André Steenbergen, Gerard E. Oosting, and Johan C. van de Grampel*

Received October 19, 1989

Novel *gem*-alkyl(hydroxyalkyl)tetrachlorocyclotriphosphazenes (**2**), $(NPCl_2)_2NPR^1C(OH)R^2R^3$ (R^1 = CH_3, *i*-C_3H_7, *t*-C_4H_9; R^2 = H, CH_3; R^3 = CH_3, C_2H_5, C_6H_5, C_6H_4-*o*-NO_2, C_6H_4-*o*-OCH_3, cyclic C_4H_3O, $COOC_2H_5$, CH_2Cl, $CH{=}CHCH_3$, C_6H_4-*p*-$CH{=}CH_2$, η^5-C_5H_4-Fe-η^5-C_5H_5; R^2-R^3 = -$(CH_2)_5$-), have been synthesized in moderate to high yields via the nucleophilic addition of phosphazenocuprates, $[(NPCl_2)_2NPR^1]_2CuMgX{\cdot}(n\text{-}C_4H_9)_3P$, to aldehydes and ketones followed by acid hydrolysis. The proton-decoupled ^{31}P NMR spectra of compounds with $R^2 \neq R^3$ show patterns typical of AXY spin systems, allowing determination of coupling constants between PCl_2 groupings. A proof for the assignment of the spin system was obtained from proton-decoupled homonuclear ^{31}P shift-correlated 2-D NMR spectroscopy. A new structure for the phosphazenocuprate is proposed. In this structure copper is coordinated onto a phosphorus center, whereas magnesium is linked to a ring nitrogen.

Introduction

In the past decade the organic chemistry of phosphazenes has been greatly enlarged. Organophosphazenes are now being applied in medicinal chemistry,[1-3] organometallic chemistry,[4,5] and polymer chemistry.[6-10]

In the field of organometallic and hybrid organic-inorganic polyphosphazenes, the need arose for cyclophosphazenes, derived from the readily available $(NPCl_2)_3$ (**1**), bearing but one reactive

(1) Van der Huizen, A. A. Aziridinyl Cyclophosphazenes: Synthesis, Structure and Cytostatic Activity. Ph.D. Thesis, University of Groningen, 1984. Van der Huizen, A. A.; Wilting, T.; van de Grampel, J. C.; Lelieveld, P.; van der Meer-Kalverkamp, A.; Lamberts, H. B.; Mulder, N. H. *J. Med. Chem.* **1986**, *29*, 1341.
(2) Mulder, N. H.; Meijers, W. H.; van der Meulen, J. D.; Sleijfer, D. T.; Uges, D. R. A.; de Vries, E. G. E.; Postmus, P. E.; van de Grampel, J. C.; Willemse, P. H. B. *Cancer Treat. Rep.* **1987**, *71*, 155.
(3) Postmus, P. E.; Mulder, N. H.; van de Grampel, J. C.; Meijers, W. H.; Berendsen, H. H. *Eur. J. Cancer Clin. Oncol.* **1987**, *23*, 1207.
(4) Allcock, H. R.; Desorcie, J. L.; Riding, G. H. *Polyhedron* **1987**, *6*, 119.
(5) Allcock, H. R.; Mang, M. N.; McDonnell, G. S.; Parvez, M. *Macromolecules* **1987**, *20*, 2060.
(6) Neilson, R. H.; Wisian-Neilson, P. *J. Macromol. Sci., Chem.* **1981**, *A16*, 425.
(7) Fieldhouse, J. W.; Graves, D. F. *ACS Symp. Ser.* **1981**, *171*, 315.
(8) Allcock, H. R. *J. Polym. Sci., Polym. Symp.* **1983**, *No. 70*, 71.
(9) Allen, C. W.; Bright, R. P. *Macromolecules* **1986**, *19*, 571.
(10) Dhathathreyan, K. S.; Jekel, A. P.; van de Grampel, J. C. *J. Chem. Soc., Dalton Trans.* **1988**, 1099.

0020-1669/90/1329-2658$02.50/0